SSRG International Journal of Geo-informatics and Geological Science
ISSN: 2393–9206 / https://doi.org/10.14445/23939206/IJGGS-V12I1P103

Volume 12 Issue 1, 23-37, Jan-Apr 2025

Original Article

Geochemical Characteristics of Stream Sediments and Rocks for Gold Mineralization Potential Around Okeigbo-Epe and Its Environs, Southwestern Nigeria

Kouame Saint Blanc Kouassi[1], Isibor Roland[2], John Ogbole[3], Abdou wahidou Seidou[4]

[1]*Mineral Exploration program, Pan African University Life and Earth Institute (Including Health and Agriculture), Ibadan, Nigeria.*
[2]*Department of Earth Sciences, Ajayi Crowther University, Oyo, Nigeria.*
[3]*National Space Research and Development Agency (Obasanjo Space Centre), Abuja.*
[4]*Pan African University Life and Earth Institute (Including Health and Agriculture), Ibadan, Nigeria.*

Corresponding Author : kouamsaintblanc@gmail.com

Received: 29 January 2025 Revised: 01 March 2025 Accepted: 15 March 2025 Published: 30 March 2025

Abstract *- This study investigates the potential for gold mineralization around Okeigbo-Epe and its environs in Ondo state, southwestern Nigeria, addressing the region's limited research on gold occurrences. Landsat-9 OLI 2 was processed using the False Colour Composite technique for lithology and lineament mapping. Geological field mapping was carried out, and 5 rock samples and 20 stream sediments were collected. Geochemical analysis of stream sediments and rock samples was performed using Inductively Coupled Plasma Mass Spectrometry and Instrumental Neutron Activation Analysis (ICPMS-INAA) for major oxides and trace element determination. Key findings include the occurrence of NE-SW, NNE-SSW, and NW-SE trending lineament indicative of tectonic activity during the Pan-African orogeny. The Lithology within the study area includes granite, banded gneiss and quartzo-feldspathic rocks. The rock samples were highly siliceous, while the gold concentration was low (<5ppb). The R-mode Factor analyses indicate the presence of sulfur minerals, Zircon, and monazite. Pathfinders like Co (3-23ppm), Cu (9-19ppm), Pb (12-22ppm), and Zn (10-94ppm) were found in noticeable concentrations. La (1.6-182ppm) and Ce (5-317ppm) anomalies were found, indicating a promising area for REE exploration. Integrating remote sensing and geochemical data proved effective in characterizing the area's geology and lineament structures, trace element geochemical signature, and mineralization potential.*

Keywords *- Gold, Landsat-9 OLI (2), False colour Composite Technique, Lineament mapping, Mineralization potential, Okeigbo-Epe Southwest Nigeria.*

1. Introduction

The implementation of renewable and green energy technology requires the availability of some critical metals such as gold (Au), silver (Ag), platinum (Pt), nickel (Ni), copper (Cu), REE, cobalt (Co), etc. [1]. A gold reserve is a symbol of wealth for countries, and its applications are found in areas such as monetary exchange, jewellery, allied wares, and dentistry, as well as as a component in the manufacturing of some electronic devices. Gold mining represents a relevant sector likely to generate wealth and favour sustainable socio-economic development for a nation. Due to its paramount importance, countries worldwide are interested in acquiring gold through purchasing or initiating exploration programs in view of discovering economically minable gold deposits. Several studies have been undertaken in Nigeria to assess the country's potential for gold**.** Gold occurrences are essentially located in the western half of the country in a favourable geologic environment, known as the Nigerian schist belts, as primary mineralization within quartz veins or as alluvial/eluvial deposits [2, 3,4,5,6]. [7] revealed that about 90% of Nigeria's total gold production has been from alluvial deposits derived from primary gold mineralisation in the basement rocks.

The Ilesha schist belt in the country's southwestern part is equally important concerning gold occurrences [8, 9, 10f]. Other places in the southwestern area have been investigated and proven to host gold occurrences, such as Osu–Amuta–Itagunmodi [11, 6].

Surficial exposure of primary deposits undergoes alteration, erosion, and accumulation in alluvial or eluvial drifts as secondary ore deposits. The latter can constitute high-grade, profitable deposits. Artisanal mining tends to focus on secondary deposits because they are more accessible.

Artisanal miners have performed ground scavenges around Okeigbo-Epe's and its environs.

However, the geochemical characterization of placers at a small scale around that locality has not been studied yet. The lack of research regarding the geological and geochemical characterization of these deposits limits the optimal exploitation of the mineralization and most often results in the abandonment of these gold sites.

This research contributes to understanding Okeigbo-Epe's and the environment's geological framework and mineral potential in southwestern Nigeria, offering a foundation for sustainable mineral exploration and development initiatives.

The investigated area is located in Ondo State, southwest Nigeria, between longitudes 4°44′9.03″E and 4°48′14″E and latitudes 7°12'0.05''N and 7°7'12.38''N (Figure 1). It represents a small fraction of the schist belts in southwestern Nigeria.

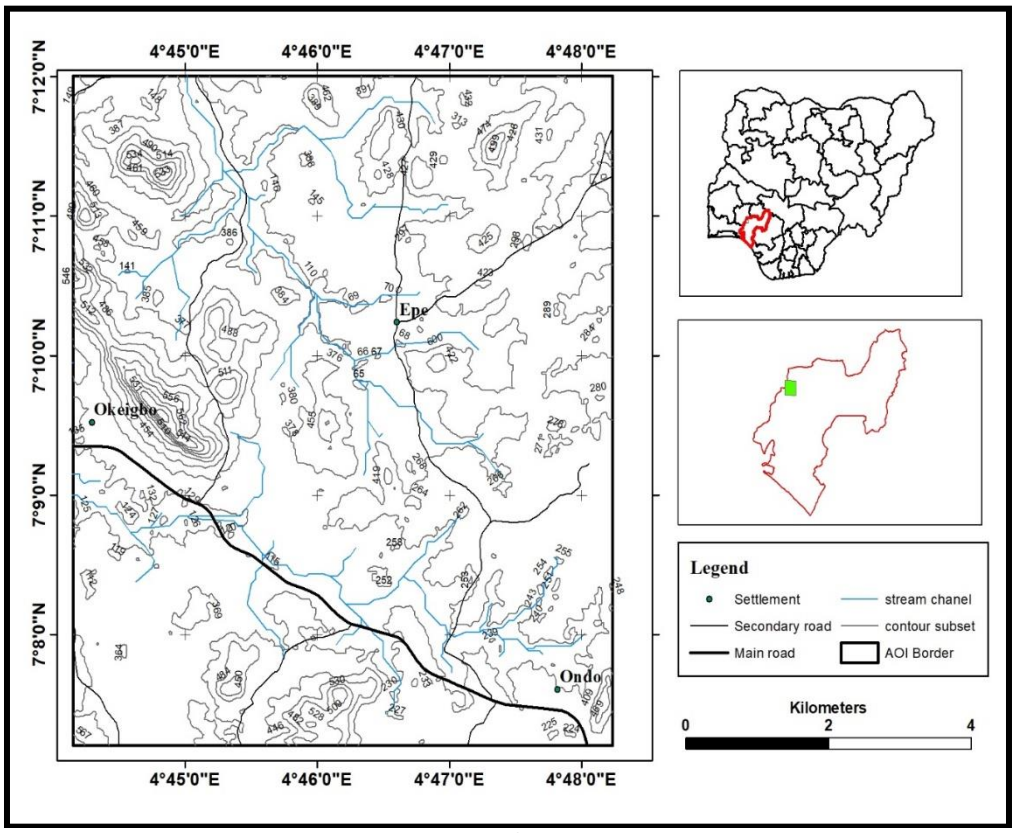

Fig. 1 Location of the study area

2. Regional Geological Setting

Nigeria is situated in the West African sub-region. The geochronological dating carried out reveals that Nigeria's geology results from four major orogeneses: the Liberian (2700 Ma), the Eburnian (2000 Ma), the Kibaran (1100 Ma), and the Pan African orogeny (400 Ma) [12,13,14,15,7]. The study area is part of the Nigerian Basement Complex within the Ilesha schist belt.

The schist belt is one of Nigeria's basement complex's four major geological units [7]. The Older Granites (Pan African granitoid), the Migmatite – Gneiss Complex (MGC) and the Undeformed Acid and Basic Dykes constitute the three other geological constituents of the Basement complex of Nigeria [7]. Considered to be Upper Proterozoic supracrustal rocks that have been infolded into the migmatite-gneiss-quartzite complex, the schist belts are a set of metasediment and metavolcanic rocks that lie essentially in the western half of Nigeria with an N-S direction [5,7]. However, few are localized in central Nigeria [16,17] and further to the eastern part of the country [18].

The Ilesha-egbe and Iperido schist belts in southwestern Nigeria are favourable areas to explore for gold, as witnessed by the small-scale mining activities that have been reported [6,11]. Furthermore, remote sensing has also proved useful for geological mapping and identifying fractured zones and hydrothermal alteration [19,20]. Space data in southwest Nigeria allows mapping of the geology, the lineaments, and hydrothermal alteration [8]

Nonetheless, ground surveys backed with geochemical analysis remain more efficient in providing relevant data about rocks' petrological features, mineralogy content, and grade of major and trace elements. With the improvement of mineral exploration methods and sample analytical technologies, it is possible to cover a large area and detect the low concentration of trace elements, including gold, in collected samples.

Underexplored areas remain important in the southwestern provinces of Nigeria. Previous works suggest other deposits have yet to be discovered in southwest Nigeria [7]. Therefore, This research work aims to study and unravel the geochemical traits of geological materials at Okeigbo-Epe, within the Ilesha schist belt, to assess its mineralization potential.

2.1. Local Geology

The digitized map was derived from the geological map of Ondo state. Gneiss and undifferentiated migmatite cover the majority of the study area. Granodiorite and granite rock intrude on the migmatite. Quartzite and quartz schist underlie the northeastern part of the study area, while quartzofelspathic granulite is confined to the western part of the study area (Figure 2).

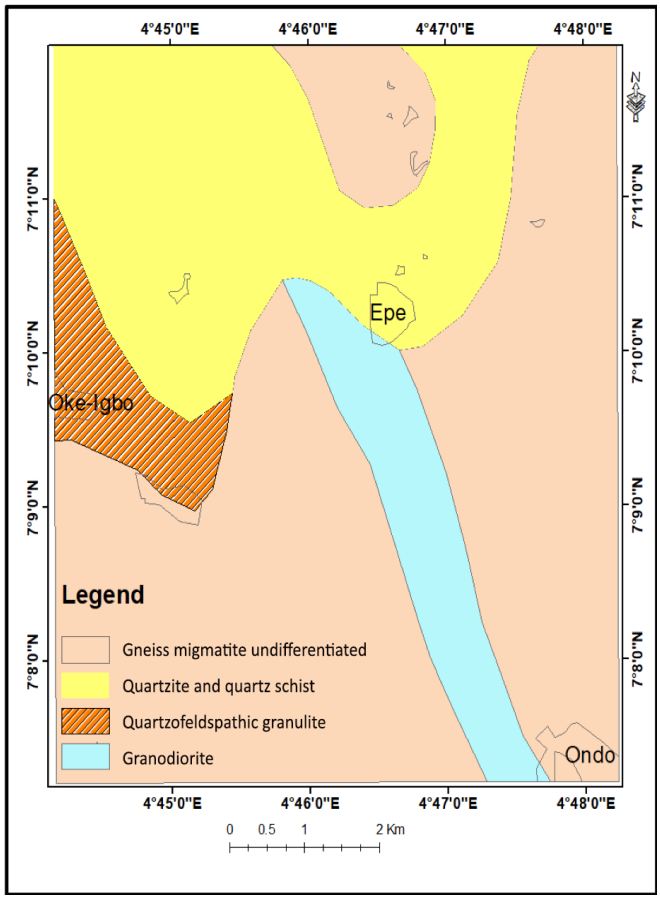

Fig. 2 Geological map of Okeigbo-Epe digitized in arcmap 10.8 after NGSA (2006)

3. Methodology

3.1. Landsat Image Processing

A Landsat-9 OLI 2 image corresponding to row and path p190r55 acquired on 13/01/2023 was downloaded from the USGSS website and processed to map lineament features.

The Fast Line-of-sight Atmospheric Analysis of Spectral Hypercubes (FLAASH) algorithm in ENVI software helped convert the Landsat-9 image to surface reflectance, followed by the sub-setting of the study area. During atmospheric correction, the raw radiance and digital number data from the imaging spectrometer are converted into reflectance data.

The resulting spectra can be directly compared with laboratory or field reflectance spectra. Contrast and edge enhancement filters were applied to improve the image's visual clarity. This study did not utilize the bands of the panchromatic and cirrus clouds (Band 9). The different composite image was performed. The lineaments were digitized manually, and a rose plot was created to visualize their lengths and orientations.

3.2. *Fieldwork* and Sample Preparation

Geological fieldwork consisting of rock outcrops description and sample collection was carried out in the Study area. 5 rock samples and 20 stream sediment samples were collected.

The sampling points are presented in Figure 3. The samples were collected randomly along a river channel at a depth of 1m and kept in a polyethene bag. Care was taken to avoid contamination.

The loose stream sediment samples were dried in the open air and sieved to remove organic matter and a fraction less than 0.63 micrometres were taken for analysis. The rocks and stream sediment samples were submitted to ICPMS-INAA code 4E at the Activation Laboratory (ACTLAB) Canada to determine their major element and trace element composition. The choice of this analytical method (ICPMS-INAA) is justified by its capacity to analyze the gold content in the sample.

3.3. Data Analysis

The geochemical data were subjected to descriptive statistical analysis. The range, mean, and standard deviation of each variable were determined. To facilitate the interpretation of the data, a comparison with regard to the Upper Continental Crust values according to [21] was done.

Principal component analysis was done using the concentration of trace elements to reduce the length of variables and unravel latent mineralogical associations within the data set. The statistical GraphPad Prism software was used for the principal component analysis and some plots.

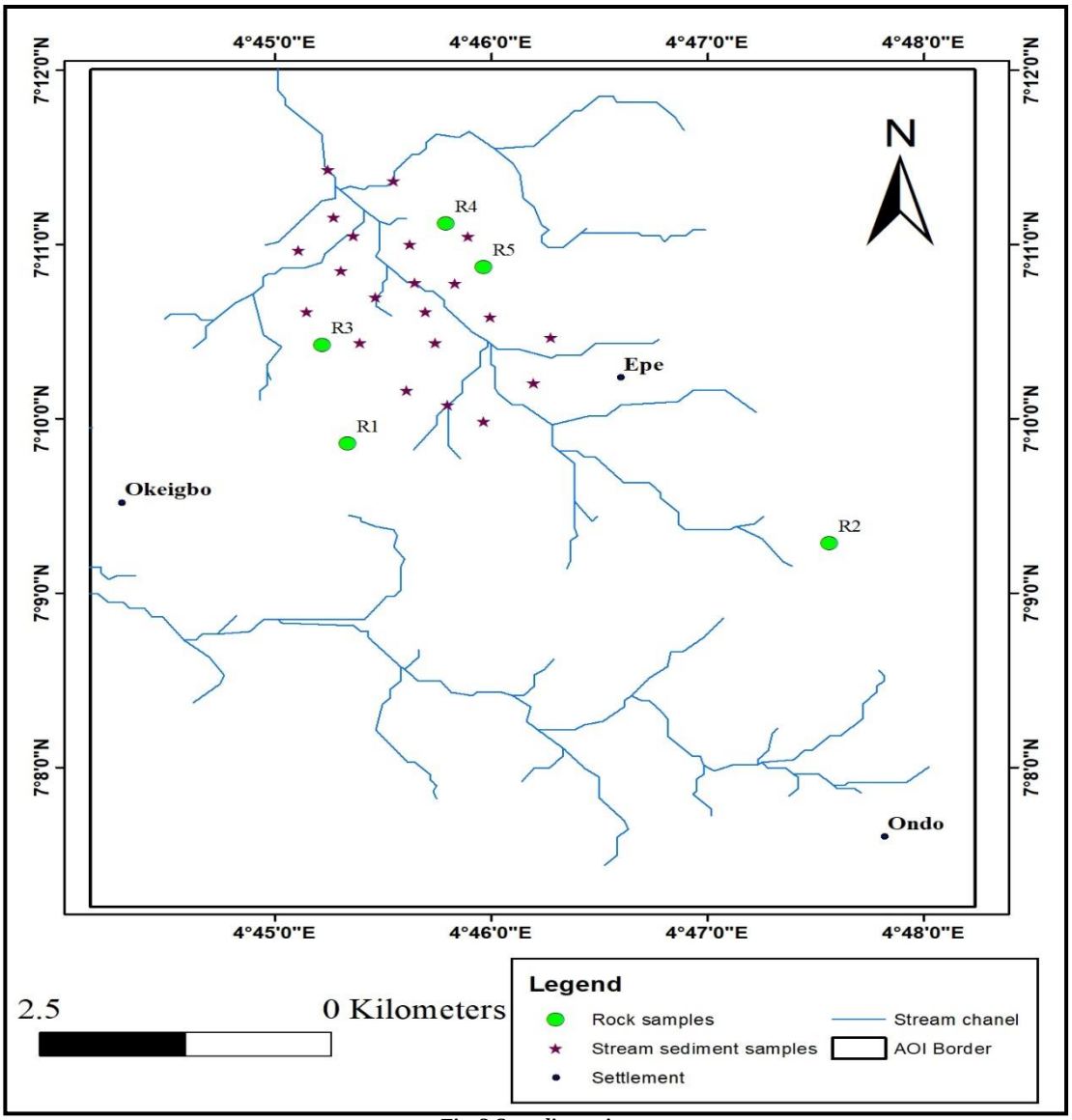

Fig. 3 Sampling points map

4. Results and Discussion

4.1 Satellite Image Analysis

4.1.1. Composite Maps

Various false colour composite models were developed for Landsat-9 OLI data over the study area. Based on their correlation coefficients, the models combined the least correlated bands into Red, Green, and Blue (RGB). The resulting colour composites (Figure 4) revealed varying levels of information.

Proper interpretation of these composites often requires experience and background knowledge, as factors such as texture, tone, pattern, association, and size of image elements were considered during the analysis. The OLI band 762 composites also highlighted the major structural trends distinctly differentiated in this composite.

4.1.2. Lineament Trend Analysis

Multispectral images are regarded as much more efficient tools for discerning lineaments because they are acquired through variable wavelength intervals of the electromagnetic spectrum [22]. The main linear structures in the OLI band 762 composites were distinguishable, and lineaments were derived from this composite (Figures 6 and 7). These structures were then plotted on an orientation rose diagram, with the most prominent trend being NNE – SSW, a few NW – SE and E – W trending structures (Figure 8). The frequency of the structural trend is described in Figure 9. The lineaments have a maximum length of 1.5 km, a minimum length of 25 m, and a mean length of 805 m. The Rose diagram produced from the lineaments shows that the dominant orientation is NE-SW with (56.87%) lineaments. Minor orientations are NNE-SSW with (17.06%) lineaments, NW-SE with (22.27%) and E-W with (3.791%) and N – S.

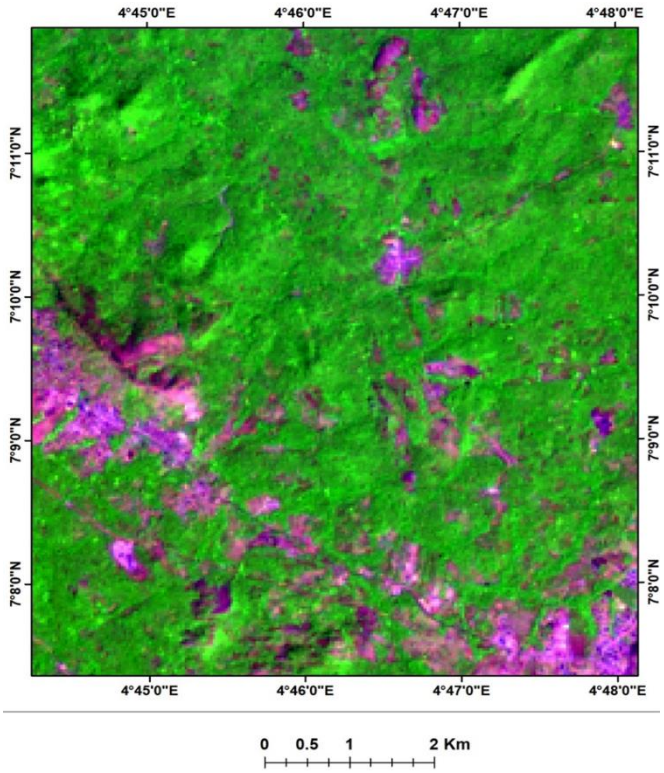

Fig. 4 Red, Green and Blue 652 colour composite of Landsat 9 OLI of the study area showing vegetation intensity in green and settlements in a purplish colouration

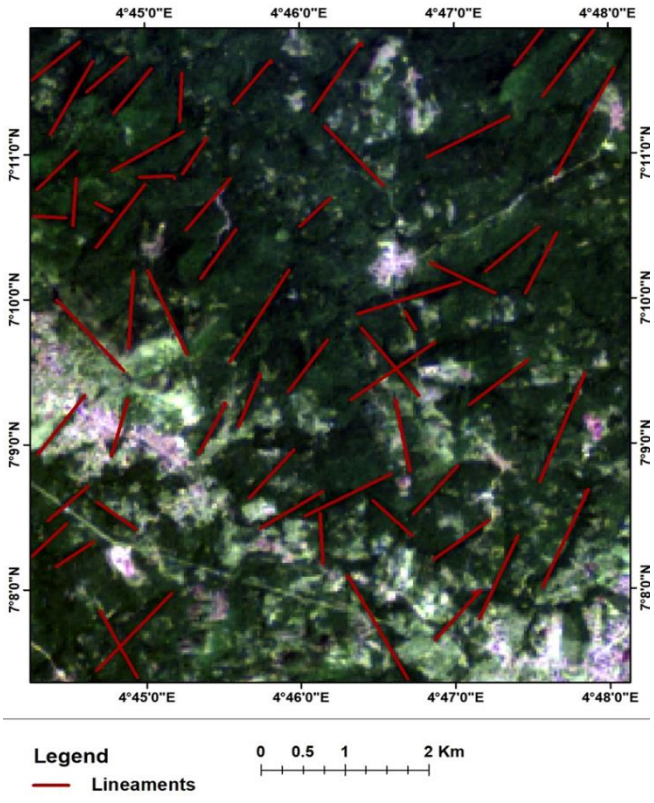

Fig. 6 Red, Green, and Blue 762 colour composite of Landsat 9 OLI of the study area with Lineaments overlayed

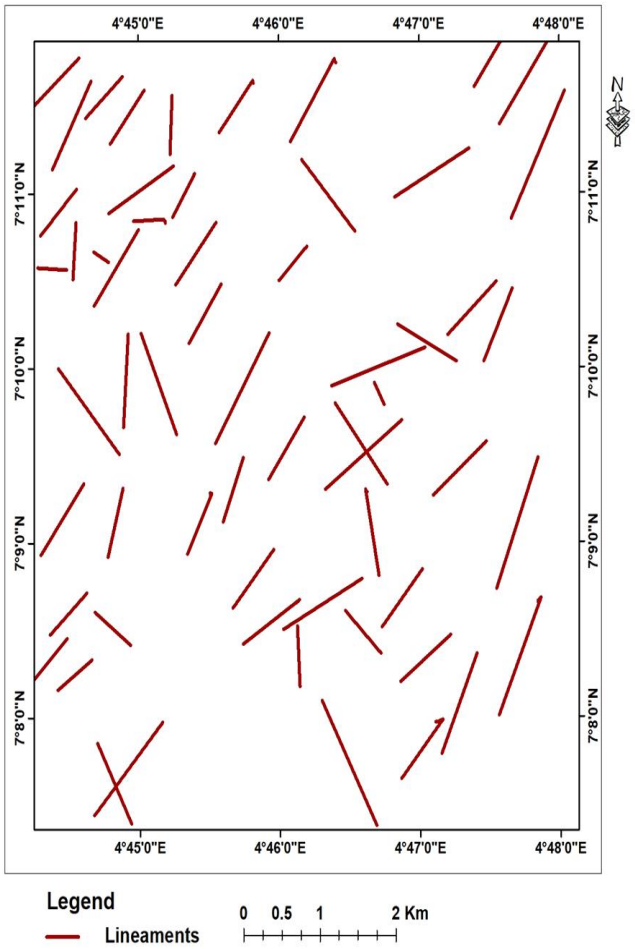

Fig. 7 Lineament map derived from Red, Green, and Blue 762 colour composite of Landsat 9 OLI of the study area

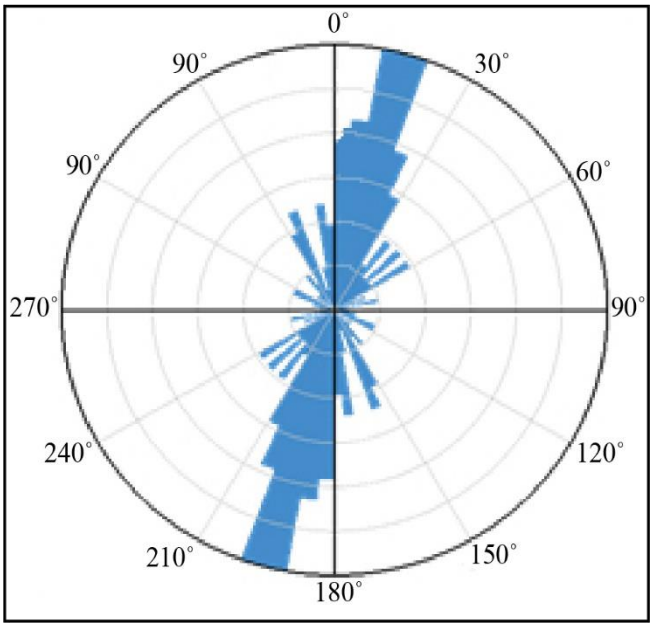

Fig. 8 Rose diagram of the lineaments

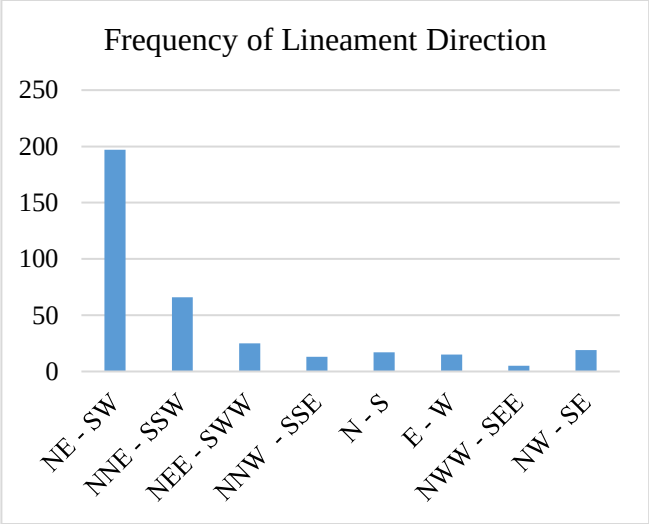

Fig. 9 Histogram of predominant lineament direction

4.2. Geochemistry Analysis

4.2.1. Lithology

The study area falls into the Nigerian Precambrian Basement Complex of southwestern Nigeria. The principal rock types encountered in the study area include Granite, Banded gneiss, and pegmatite. Granite and Banded gneiss are the major rock types, while pegmatite represents the minor rock.

The Granite

It occurs as low-lying and hilly outcrops. It covers the western part of the study area. A hand specimen shows a phaneritic texture with abundant quartz, potassic feldspar, mica, and biotite (Figure 10).

The Banded Gneiss

This metamorphic rock is observed on the eastern side of the study area. Surface exposures of fresh outcrops are very few due to their high susceptibility to weathering and alteration. The outcrop has a predominantly dark colouration (Figure 11). The rock is foliated and characterized by an alternation of tiny light quartzo-feldspathic minerals and dark, thicker bands of biotite hornblende minerals. It occurs as a low layering outcrop trending N°168 with a foliation plane dipping 39° toward the east.

The Pegmatite

The pegmatite bodies intrude within the granite and the banded gneiss. They occur as dykes and veins of varying dimensions. They generally outcrop as a low-lying outcrop. Its length varies from a few centimetres to 8 meters around Popoola Ehinoke Okeigbo. Figure 12 shows a pegmatite intrusion in the granite. Weathering and erosion favoured the deposition of the pegmatite and granite constituents into the stream channel, where gold occurrences are suspected for this study.

Fig. 10 Field photograph of granitic outcrop around Okeigbo-Epe (N 07’09’364’’, E 004’46’4461)

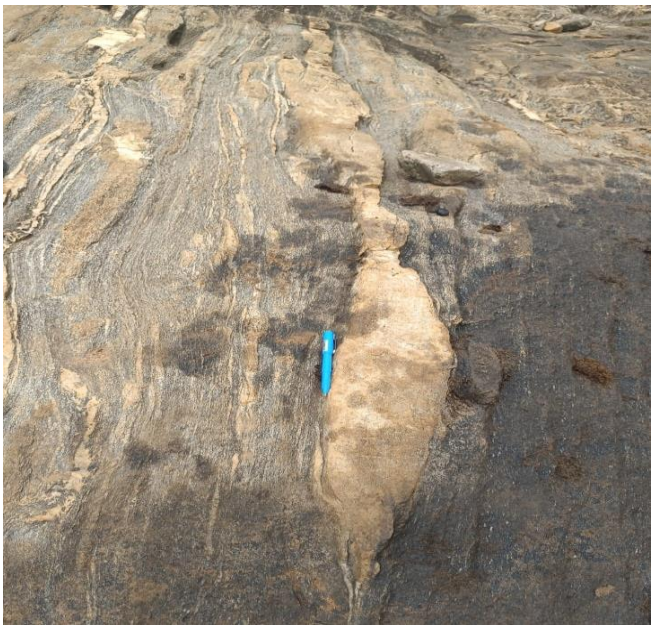

Fig. 11 Field photograph of a banded gneiss showing mineral lineation (07’08’853’’N, 004’47’289 E)

Fig. 12 Field photograph showing pegmatite intrusions within the granite outcrop outcrops

4.2.2. Stream Sediment Chemistry

The results of the geochemical analysis of the major oxide of the stream sediment samples are recorded in Table 1. The results show a high concentration of SiO2 among the set of analyzed samples. SiO2 concentration ranged from 67.35 to 97.41 wt.%, with a mean value of 91.35 wt.%. This can be ascribed to the felsic nature of the outcrops within the study area. The oxide percentages of Al2O3 (1.31-13.22 wt.%) and Fe2O3 (1.02-8.53 wt.%) have a mean of 3.23 and 1.96 wt.%, respectively. Their concentrations vary significantly among the samples.

The high proportion of SiO2 and the moderate proportion of Al2O3 and Fe2O3 can be related to the expressed presence of quartz, plagioclase, sodium feldspar, and iron oxide minerals. MnO concentration ranged from 0.01 to 0.06 wt.%, with a mean value of 0.02 wt.%, which is higher than its value (0.01 wt.%) in the UCC. MgO (0.02-2.38 wt.%) and CaO (0.03-1.55 wt.%) concentrations show a narrow variation to their respective mean value of 0.22 wt.% and 0.07 wt.%. There is a depletion of MgO and CaO compared to their UCC values (2.48 and 3.59). Na2O (0.04 - 0.46 wt.%) and K2O (0.53 and 2.93 wt.%) have oxide percentages that show a narrow variation, as corroborated by their low standard deviation value of 0.11 and 0.71, respectively. The average value of Na2O is 0.154 wt.% and is 1.00 wt.% for K2O. TiO2 (0.04-1.046) has an average of 0.35, while that of P2O5 (0.01-0.07) is 0.02 wt.%. The Lost on Ignition (LOI) values range from 0.27 to 4.94, with a mean value of 0.91. This shows that the sample has a low volatile mineral content and a low content of organic matter.

Trace element concentration values in part per million (ppm) except gold (in part per billion ppb) are presented in Appendix 1 and 2.

Table 1. Major composition of the stream sediments

Analyte Symbol	SiO_2	Al_2O_3	Fe_2O_3(T)	MnO	MgO	CaO	Na_2O	K_2O	TiO_2	P_2O_5	LOI	Total
K1	97.41	1.31	1.02	< 0.01	0.04	0.06	0.1	0.63	0.04	< 0.01	0.33	100.9
K2	96.74	1.46	1.26	0.01	0.03	0.05	0.11	0.59	0.256	< 0.01	0.41	100.9
K3	94.44	1.76	1.57	0.02	0.02	0.06	0.14	0.72	0.345	0.03	0.43	99.54
K4	93.8	1.47	1.52	0.01	0.02	0.04	0.1	0.65	0.112	< 0.01	0.32	98.06
K5	93.75	2.04	1.25	0.01	0.02	0.06	0.15	0.87	0.153	< 0.01	0.49	98.8
K6	95.6	1.83	1.21	0.01	0.03	0.06	0.13	0.81	0.136	0.01	0.4	100.2
K7	94.28	1.89	1.3	0.01	0.02	0.07	0.15	0.87	0.275	0.02	0.27	99.15
K8	95.55	1.86	1.69	0.02	0.03	0.06	0.11	0.66	0.542	0.03	0.37	100.9
K9	67.35	13.22	8.53	0.06	2.38	0.03	0.14	2.96	1.046	0.03	4.94	100.7
K10	94.81	1.71	1.35	0.02	0.02	0.05	0.11	0.74	0.471	0.02	0.42	99.74
K11	85.18	6.6	2.47	0.01	0.4	0.03	0.04	0.53	0.404	0.03	2.89	98.59
K12	92.74	3.43	1.51	0.05	0.19	0.21	0.31	1.1	0.279	< 0.01	0.44	100.3
K13	93.26	2.24	1.36	0.01	0.03	0.07	0.17	0.81	0.25	0.02	0.42	98.65
K14	88.73	4.85	2.16	0.04	0.3	0.12	0.16	1.39	0.588	0.05	1.65	100
K15	81.61	7.41	3.74	0.03	0.62	0.2	0.46	2.55	0.505	0.03	1.49	98.65
K16	93.74	3.19	1.39	0.02	0.05	0.1	0.19	1	0.318	0.03	0.89	100.9
K17	94.65	1.5	1.65	0.03	0.03	0.05	0.1	0.54	0.56	0.07	0.35	99.54
K18	96.21	1.67	1.19	< 0.01	0.04	0.06	0.12	0.69	0.113	< 0.01	0.41	100.5
K19	92.12	3.18	1.72	0.02	0.17	0.09	0.16	1.11	0.367	0.02	0.69	99.65
K20	94.74	2.08	1.44	0.02	0.05	0.08	0.13	0.85	0.268	0.01	0.61	100.3
Min	67.35	1.31	1.02	0.01	0.02	0.03	0.04	0.53	0.04	0.01	0.27	
Max	97.41	13.22	8.53	0.06	2.38	0.21	0.46	2.96	1.046	0.07	4.94	
mean	**91.84**	**3.24**	**1.97**	**0.02**	**0.22**	**0.08**	**0.15**	**1.00**	**0.35**	**0.03**	**0.91**	
SDV	8.15	3.37	2.03	0.02	0.66	0.05	0.11	0.71	0.26	0.02	1.33	
UCC	66.6	15.4	**5.04**	0.1	**2.48**	**3.59**	**3.27**	**2.8**	**0.64**	**0.15**		100.05

Trace elements such as Au (<5ppm), Ag(<0.5ppm), As(<2ppm), Bi(<2ppm), Br(<1ppm), and Cd (<0.5ppm), Hg (<1), Ir(<5), Mo(<2) have concentrations below the detection limit of the analytical method used.

Large Ion Lithophile Elements (LILE) such as Rb (30-190ppm), Ba (136-500ppm), and Sr(11-80ppm) show high values in some samples compared to Cs (0.5-8.2) and Be (1-3ppm). Cesium (Cs) is reported in a few samples, such as K6 (0.5ppm), K9 (8.2ppm), K11(2.7ppm), and K15(0.5ppm). The transition metals are Cr, Ni, Co, Cu, Zn, and V. Cr (7-112ppm) and Cu (5-24ppm) were detected in all samples with an average concentration of 25.2 ppm for Cr and 9.5 ppm for Cu. The concentration of Co ranges from 1 to 37 ppm and is detected in only a few samples, including K9 (37ppm), K10 (2 ppm), K11 (4 ppm), and K15 (9 ppm) and 9.5 ppm for Cr. Zn (7-116 ppm) has an average value of 22.5 ppm. V(6-94ppm), Ni (4 - 49ppm). The concentrations of other trace elements, such as Hf (2.2-9ppm, Y (4-184ppm), Zr (70-361ppm), Th (1.5-137ppm), and U (1.3-15.2ppm), are noticeable compared to the others. REE concentrations in the table are remarkable. A comparison of these concentrations to their value in the upper continental crust (UCC) shows a very significant REE enrichment, in particular Y (4-184 ppm), La (6-266 ppm), Ce (11-534 ppm) and Nd (7-186 ppm).

4.2.3. Rock Samples Chemistry

The geochemical results of the rock samples' major oxides are presented in Table 2. The concentrations of SiO_2 range from 55.2 to 97.01 wt.%, with a mean value of 80.24 wt.%. This value shows their enrichment in Silicium compared to its value in the Upper Continental Crust (UCC) value. The concentration of Al_2O_3 shows a wide variation amongst samples, with values ranging between 0.28 – 17.44 wt.% and a mean concentration of 7wt.%, which is lower than its Clarke value. The concentration of Fe_2O_3 varies from 1.7 to 7.63 wt.% among the Lithology analysed, with a mean value of 3.93 wt.%. MnO (0.01 - 0.14 wt.%) and TiO_2 (0.031 - 0.77 wt.%) are less enriched than their UCC concentration. K_2O (0.02–5.17 wt.%) and Na_2O (0.06 –2.86 wt.%) concentrations are low and show a narrow variation with a mean value of 1.61 for K_2O and 1.6 wt.% for Na_2O. The contents of CaO (2.44-6.95 wt.%) and MgO (0.06 – 2.86 wt.%) varied widely among samples. P_2O_5 (0.27 - 0.31 wt.%) with a mean value of 0.29 and a standard deviation value of 0.02 portrays a narrow variation among samples. Regarding the UCC concentration, which represents their Clarke value, the rock is enriched in SiO_2 and P_2O_5 and depleted in the other oxides. A general increase is observed with the major oxide concentration as the SiO_2 concentration decreases. Meanwhile, rocks with high SiO_2 concentrations display a lower oxide amount.

The concentration of trace elements of the rock samples is presented in Appendix 3, along with the range, the mean and their concentration in the Upper Continental crust (UCC) [19]. Large Ion Lithophile Elements (LILEs) such as Ba (10-1400ppm), Sr (72-431ppm), Be (2-3ppm), and Rb (30-270ppm) show a general enrichment in the set of rock samples as compared to their UCC value. Being incompatible element, their affinity for the magma phase during petrogenesis Favor their concentration in the residual melt and forms silicate minerals such as Biotite, K-felspar, plagioclase, and muscovite.

Other lithophile elements such as Hf (5.1-15.6ppm), Sc (0.4-19ppm), Th (09-30.4ppm), V(10-121ppm), and Zr (31-760ppm) are noticeable. Compared to their mean value UCC, there is a light enrichment in Th and Hf in the granite and the gneiss.

Siderophile elements such as Co(3-23ppm), Ni (6-7ppm), and Cr (8-65 ppm) have low concentrations as compared to their UCC value. The concentrations of Cu (9-19ppm), Zn(16-94ppm), and Pb (12-22ppm) are noticeable, except for Sulphur (S). Additional chalcophile elements like Ag, Hg, Cd, As, and Se are below the detection limit. This can be ascribed to a depletion in sulphur-loving minerals. The multi-element plot normalized to the primitive mantled depicts trace element abundance in the set of analyzed rocks.

The enrichment in trace elements in the granite and the gneiss is more conspicuous than in the pegmatite and the quartz veins. There is a notable amount of Light Rare Earth Elements (LREE) (La, Ce, Nd). LREE ranges approximately between 6.6 and 630 ppm, while Heavy Rare Earth Elements (HREE) (Eu, Sm, Y, Tb, Yb, Lu) concentration is low (<0.05-11.18). (∑REEs) concentrations ranging from 6.9 to 668.58 ppm among samples. Both LREE and HREE of the analysed Rare Earth elements are enriched in terms of their concentration in the UCC.

4.2.4. R-mode Factor Analysis

R-mode factor analysis is a multivariate statistical technique used to identify relationships among variables. This technique helps reduce their complexity by grouping them into underlying factors or components based on their mutual correlation coefficient. Consequently, this work has been adopted. Factor analysis was used to analyze the inter-elemental relationships and groupings, and only variables with loadings greater than 0.50 were considered significant members of a particular factor component (Table 3).

Factor 1: Cu, Pb, Ta, Th, U, V, REE

Factor 1 explains 42.61% of the system variances. These factors reflect a common felsic source and the presence of felsic mineral rich. The loading factor is high (0.705-0.94) for Th, U, Ta, and the REE. This could indicate minerals such as monazite, Urinite, etc.

Factor 2: Ba, Be, Co, Cr, Cs, Sc, Rb, Ni

Factor 2 accounted for 34.57% of the total system variance and has a negative factor loading. The grouping of

Ba, Be, Co, Cr, Cs, Sc, Rb, and Ni indicates that a common mineralogical or geological factor influences those elements. Those elements could have derived from the weathering of mafic to intermediate rocks. Cr, Co, and Ni are linked to ferromagnesian minerals, while Ba, Rb, Cs, and Sc are often associated with feldspars, mica, or clay minerals. This grouping may reflect processes like mechanical erosion, Chemical weathering, or hydrodynamic sorting of the stream sediment.

Factor 3: Ba, Hf, Sr, Zr

F3 has positive factor loadings on Ba, Hf, Sr, and Zr. This could be ascribed to a mineralogical control, with heavy minerals such as Zircon derived from felsic igneous rock. Heavy minerals tend to resist weathering. On the other hand, Sr and Ba are often linked to feldspar or carbonate phases. Their grouping could indicate a sediment sorting process that concentrates both resistant heavy minerals.

Table 2. Major composition of rock samples

Analyte Symbol	SiO_2	Al_2O_3	Fe_2O_3(T)	MnO	MgO	CaO	Na_2O	K_2O	TiO_2	P_2O_5	LOI	Total
R1	65.42	14.25	5.67	0.07	0.76	2.44	2.88	5.17	0.777	0.27	0.77	98.48
R2	55.2	17.44	7.63	0.14	2.86	6.95	4.84	1.15	0.701	0.31	1.21	98.42
R3	92.43	1.42	2.46	0.06	0.32	2.44	0.06	0.02	0.044	< 0.01	0.92	100.2
R4	97.01	0.28	1.7	0.01	0.06	< 0.01	0.01	0.08	0.031	< 0.01	0.02	99.21
R5	91.13	3.08	2.19	0.01	0.11	0.01	0.18	1.66	0.057	< 0.01	0.51	98.94
Min	55.2	0.28	1.7	0.01	0.06	0.01	0.01	0.02	0.031	0.27	0.02	98.42
Max	97.01	17.44	7.63	0.14	2.86	6.95	4.84	5.17	0.777	0.31	1.21	100.2
Mean	80.238	7.294	3.93	0.058	0.822	2.96	1.594	1.616	0.322	0.29	0.686	99.05
UCC	66.6	15.4	5.04	0.10	2.48	3.59	3.27	2.80	0.64	0.15	-	-

Table 3. Factor analysis showing the rotated component matrix

	PC1	PC2	PC3	PC4	PC5
Ba	0.279	**-0.659**	**0.606**	-0.289	**0.102**
Be	0.289	**-0.893**	-0.192	0.092	-0.053
Co	0.296	**-0.934**	-0.086	0.002	-0.068
Cr	**0.544**	**-0.816**	-0.067	0.043	0.057
Cs	0.257	**-0.898**	-0.272	0.157	-0.153
Cu	**0.574**	0.168	-0.624	0.087	0.015
Hf	0.48	0.301	**0.573**	**0.532**	-0.237
Ni	0.342	**-0.931**	-0.078	0.081	0.006
Pb	**0.588**	**-0.701**	0.234	-0.137	-0.05
Rb	0.33	**-0.913**	0.044	-0.113	0.151
S	0.085	-0.061	0.02	**0.512**	**0.849**
Sc	0.382	**-0.915**	-0.047	0.057	-0.054
Sr	0.119	-0.176	**0.779**	-0.519	0.199
Ta	**0.705**	0.372	-0.45	-0.246	-0.037
Th	**0.868**	0.421	0.083	-0.12	0.08
U	**0.88**	0.363	0.019	0.014	-0.049
V	0.379	**-0.905**	-0.046	0.095	-0.055
Y	**0.952**	0.24	-0.045	-0.006	0.02
Zn	0.426	**-0.881**	-0.048	0.097	-0.009
Zr	0.449	0.296	**0.586**	**0.55**	-0.215
La	**0.926**	0.37	0.032	-0.012	0.017
Ce	**0.926**	0.366	0.049	-0.042	0.028
Nd	**0.963**	0.236	-0.024	-0.008	-0.036
Sm	**0.95**	0.306	-0.003	-0.018	0.028
Eu	**0.821**	-0.033	0.201	-0.082	-0.048
Tb	**0.75**	0.426	-0.258	-0.115	0.111
Yb	**0.942**	0.272	-0.058	-0.032	0.03
Lu	**0.948**	0.233	-0.022	-0.026	0.019
Eigenvalue	11.93	9.68	2.553	1.402	0.9685
Proportion of variance	42.61%	34.57%	9.12%	5.01%	3.46%
Cumulative proportion of variance	42.61%	77.18%	86.30%	91.31%	94.77%

Factor 4: Hf, Zr, S

The inclusion of sulfur in this group denotes the involvement of sulfur-bearing minerals like sulfides or sulfates. It also gives insight into the geochemical condition that facilitates the co-deposition or preservation of Zircon.

This could have been under reducing conditions or in an environment influenced by hydrothermal activity during the emplacement of the source rock.

F5: S

The presence of (sulfur) as the last PCA's unique component denotes that sulfur variability is controlled by a unique geochemical or environmental process distinct from the other element in the data set. It accounted for 9.12 % of the total system variance with a high loading value of 0.84. This could also describe a redox-sensitive environment where sulfur precipitates.

5. Discussion

5.1. Structural Features

The processing of the Landsat-9 OLI data revealed significant structural features. The NE-SW trend is the major trend of the lineaments. This corroborates with the fractures observed during the fieldwork, which trends N 190°, N 185°, and N 60°. The dominance of the NE-SW trend suggests the impact of the Pan-African Orogeny. This is consistent with the observation by [19,23].

Furthermore, the NNE-SSW trend is associated with gold mineralization in Anka–Yauri [24] in the Malumfashi schist belt [25]. The ENE–WSW and ESE–WNW trends were found to dominate structural control potential mineralization in the Ilesha schist belt [26].

The NE-SW trend, consistent with the NNE-SSW, is a good indicator for further investigation in the study area. The analyses of the lineaments indicated variations in orientation and length, reflecting the tectonic and erosional dynamic of the area.

A careful observation of the lineament map shows an abundance of lineaments in the centre and southwest of the study area, which is dominated by magmatic rock and then dominated to the northwest by quartzite.

5.2. Source of the Sediment

The geochemical analysis of stream sediments confirmed a felsic-dominated provenance. This was evidenced by high Th/Sc and La/Sc ratios aligned with [27] and [28] findings. The trace ratios (Ts/Sc ≈ 24.84; La/Sc ≈53.78; Th/Co≈31.09) and the low concentration of Ni (≈ 47 ppm) and Cr≈25 ppm) values suggest felsic granitic to granodioritic sources rather than mafic contributions. The calculated chemical Index of Alteration values indicates moderate to intense weathering, fostering the enrichment of Al. Such a weathering trend aligns with previous studies in India [29,30].

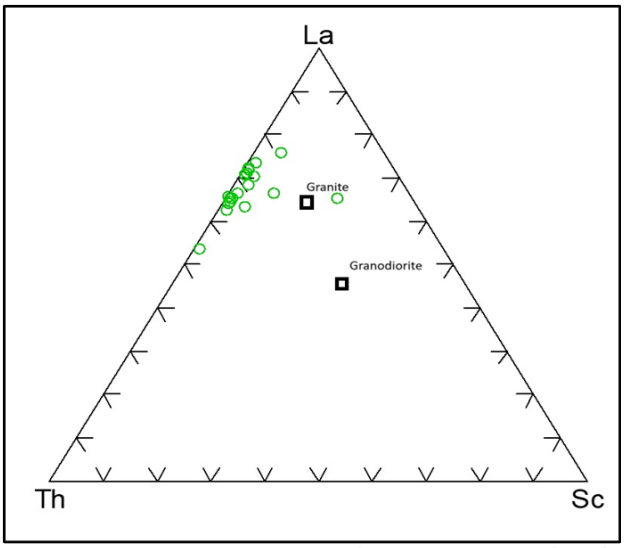

Fig. 13 La–Th–Sc showing the source of the sediment. (Modified after [27])

5.3. Mineralization Potential of the Study Area

Gold occurrences are essentially found to be associated with pathfinders such as arsenic (As), with the schist belt rock type. Gold occurs in trace quantities, generally 0.5 to 5 parts per billion (ppb) in basement rock [30]. Results showed that the concentration of gold in all analysed samples is less than 5 ppb (< 0.005 ppm). According to [31], areas with Au concentrations < 0.005 ppm are commonly barren. Also, the geochemical plots for assessing Au mineralization have 0.005 ppm as the minimum value. The gold content would be < 5ppb, which is smaller than 0.005ppm and, therefore, not of interest. Gold concentration is worth exploring depending on economic, geologic, or environmental factors. In southwestern Nigeria, trace elements such as Cu, Ag, Zn, Cd, As, Bi, Pb, Sb, W, Mo, and Se have been reported as pathfinders for gold mineralization [11,32]. Trace element shows noticeable concentrations of gold pathfinders like Co (3-23ppm), Cu (9-19ppm), Pb (12-22ppm), and Zn (10-94ppm) in the stream sediment samples. The mean values of those elements in the Upper Continental Crust show Co (25 ppm), Cu (55 ppm), Pb (14 ppm), and Zn (70 ppm), depicting a depletion of those elements. The mean values of Th (36.47ppm), U (5.51ppm), and Zr (216.85ppm) show an enrichment compared to their UCC value (165ppm, 10.5ppm), (2.7ppm). Samples (K20, K18, K15) among the stream sediment revealed significant positive anomalies in Lanthanum (La) and Cerium compared to their UCC value. That could indicate an enrichment mineralization in REE within the study area.

Combining ICPMS and INAA analytical methods for sample analysis distinguishes these results. Other authors, such as [33] (Lapworth et al., 2012) who conducted similar studies in other regions of Nigeria, only used ICPMS for regional studies. The structural study combined with the geochemical analyses proves to be a peculiar approach, especially for small-scale studies.

6. Conclusion

The fieldwork undertaken showed the presence of porphyritic granite, banded gneiss and quartz-felspathic rocks**.** The longest lineament is 1.6 km, with a minimum length of 25 m and a mean length of 805 km. The NE-SW was the lineament's dominant orientation, followed by the NNE-SSW, NW-SE, E-W, and minor N-S. The dominance of the NE-SW lineaments suggests the widespread effect of the Pan-African orogeny within the study area. The Pan-African Orogeny is known for being the latest orogeny that favoured granitoid intrusion within the metasedimentary schist belt and some mineralization, such as gold [9f]. The focus was on the stream channel environment suspected to host alluvial gold mineralization. It has been reported that the essential of gold production in Nigeria has been from alluvial deposits due to secondary ore deposits.

The results show that the area is not mineralized in gold. Nonetheless, the stream sediment and the rock samples contain Lanthanum (La) and Cerium (Ce) geochemical anomalies. This could serve as an indicator for REE exploration in the study area. The factor analysis applied to the stream sediments' trace elements reveals a latent pattern regarding element affinity. Factor 1 (Cu, Pb, Ta, Th, U, V, REE) shows a strong felsic-rich lithology. Factor 2 (Ba, Be, Co, Cr, Cs, Sc, Rb, Ni) denotes ferromagnesian-rich minerals, and Factor 3 (Ba, Hf, Sr, Zr) underlies heavy minerals such as zirconium.

In contrast, factors 4 (Hf, Zr, S) and 5 (S) depict sulfur-rich minerals and redox-sensitive environments where sulfur precipitates rocks derived from a mafic melt that undergoes differentiation as minerals precipitate. Advanced geophysical methods should be implemented to further enhance the understanding of the mineralization in the study area. Induced polarization, which measures the earth's electrical potential, can help delineate additional sulfur-rich metals. Furthermore, increasing the number of rock samples collected from the area will provide more comprehensive geochemical and petrographic information.

Conflicts of Interest

The authors confirm that this research was conducted independently, without any commercial or financial ties that could present a potential conflict of interest.

Funding statement

The African Union funded the geochemical analysis in this work through the Pan African University Life and Earth Science Institute (Including Health and Agriculture).

Acknowledgements

The authors would like to thank the African Union Commission, which, through the Pan African University Life and Earth Science Institute (Including Health and Agriculture), provided financial support for the field activities and geochemical analyses undertaken in this research. Thanks also go to all those who have contributed to improving this work.

References

[1] "*The Role of Critical Minerals in Clean Energy Transitions: Mineral Requirements for Clean Energy Transitions*," International Energy, Report, pp. 1-287, 2021. [Publisher Link]

[2] Michael Woakes, M.A. Rahaman, and A.C. Ajibade, "Some Metallogenetic Features of the Nigerian Basement," *Journal of African Earth Sciences (1983)*, vol. 6, no. 5, pp. 655-664, 1987. [CrossRef] [Google Scholar] [Publisher Link]

[3] Michael Woakes, "Mineral Belts of Nigeria: A Review," *Global Tectonics and Metallogeny*, vol. 3, no. 2-3, pp. 115-123, 1989. [CrossRef] [Google Scholar] [Publisher Link]

[4] I. Garba, "Geochemical Characteristics of the Gold Mineralization Near Tsohon Birnin Gwari, Northwestern Nigeria," *Geochemistry*, vol. 62, no. 2, pp. 160-170, 2002. [CrossRef] [Google Scholar] [Publisher Link]

[5] J.A. Adelkoya, O.O. Kehinde-Phillips, and A.M. Odukoya, "Geological Distribution of Mineral Resources in Southwestern Nigeria," *Nigerian Mining and Geosciences Society (NMGS)*, pp. 1-13, 2003. [Google Scholar] [Publisher Link]

[6] Jerry O. Olajide-Kayode et al., "Assessment of Gold Mineralisation in Osu–Amuta–Itagunmodi Areas, Southwestern Nigeria," *Arabian Journal of Geosciences*, vol. 13, pp. 1-19, 2020. [CrossRef] [Google Scholar] [Publisher Link]

[7] Nuhu George Obaje, *Geology and Mineral Resources of Nigeria*, 1st ed., Springer Berlin Heidelberg, pp. 1-221, 2009. [CrossRef] [Google Scholar] [Publisher Link]

[8] Cyril Chibueze Okpoli et al., "Mineral Exploration of IWO-Apomu Southwestern Nigeria Using Aeromagnetic and Remote Sensing," *The Egyptian Journal of Remote Sensing and Space Science*, vol. 25, no. 2, pp. 371-385, 2022. [CrossRef] [Google Scholar] [Publisher Link]

[9] I.B. Odeyemi, *Lithostratigraphy and Structural Relationships of the Upper Precambrian Metasediments in Igarra Area, Southwestern Nigeria*, Precambrian Geology of Nigeria, Geological Survey of Nigeria, pp. 111-121, 1988. [Google Scholar] [Publisher Link]

[10] sNaheem Banji Salawu et al., "New Insights on the Ife-Ilesha Schist Belt Using Integrated Satellite, Aeromagnetic and Radiometric Data," *Scientific Reports*, vol. 11, pp. 1-23, 2021. [CrossRef] [Google Scholar] [Publisher Link]

[11] Michael T. Asubiojo et al., "Controlled Method of Determine Gold Mineralization Potentials in an Unexploited Area; A Case Study of Itagunmodi and Osu, Southwestern, Nigeria," *Earth Science Malaysia (ESMY)*, vol. 6, no. 2, pp. 82-92, 2022. [CrossRef] [Google Scholar] [Publisher Link]

[12] P. McCurry, *The Geology of the Precambrian to Lower Palaeozoic Rocks of Northern Nigeria. A Review*, Geology of Nigeria, Elizabethan Publishing Company, pp. 1-436, 1976. [Google Scholar] [Publisher Link]

[13] M.A. Rahaman, *Review of the Basement Geology of SW Nigeria*, Elizabethan Publishing Company, pp. 1-436, 1976. [Google Scholar] [Publisher Link]

[14] A.C. Ajibade et al., *Structural Relationships in the Schist Belts of Northwestern Nigeria*, Precambrian Geology of Nigeria, Geological Survey of Nigeria, pp. 103-109, 1988. [Google Scholar] [Publisher Link]

[15] S.S. Dada, *The Basement Complex of Nigeria and its Mineral Resources (A Tribute to Prof. MAO Rahaman)*, Proterozoic Evolution of Nigeria, Akin Jinad and Co, pp. 29-44, 2006. [Google Scholar]

[16] B.F. Emeronye, "Appraisal of Manganese Mineralization Around Ikpeshi, Bendel State, Nigeria," *Abstract of Seminar GSN*, pp. 1-5, 1988. [Google Scholar]

[17] P.O. Oluyide, and O.A. Oluyide, "Lithostructural Setting and Emplacement History of Precambrian Carbonate Deposits, Burum Central Nigeria," *Book of Abstracts 31st Annual International Conference of the Nigerian Mining and Geosciences Society, Calabar*, pp. 1-20, 1995. [Google Scholar]

[18] Barth Nwoye Ekwueme, *The Precambrian Geology and Evolution of the Southeastern Nigerian Basement Complex*, University of Calabar Press, pp. 1-135, 2003. [Google Scholar] [Publisher Link]

[19] Ayo A. Omitogun, and John O. Ogbole, "Lithologic, Hydrothermal Alteration and Structural Mapping of Okemesi Folds and Environs Using LandSat 8 OLI and ASTER DEM," *Journal of Geography, Environment and Earth Science International*, vol. 12, no. 3, pp. 1-19, 2017. [CrossRef] [Google Scholar] [Publisher Link]

[20] Wanduku Tende Andongma et al., "Mapping of Hydrothermal Alterations Related to Gold Mineralization within Parts of the Malumfashi Schist Belt, North-Western Nigeria," *The Egyptian Journal of Remote Sensing and Space Science*, vol. 24, no. 3, pp. 401-417, 2021. [CrossRef] [Google Scholar] [Publisher Link]

[21] R.L. Rudnick, and S. Gao, *3.01 - Composition of the Continental Crust*, Treatise on Geochemistry, vol. 3, pp. 1-64, 2003. [CrossRef] [Google Scholar] [Publisher Link]

[22] Antonio M Casas et al., "LINDENS: A Program for Lineament Length and Density Analysis," *Computers & Geosciences*, vol. 26, no. 9-10, pp. 1011-1022, 2000. [CrossRef] [Google Scholar] [Publisher Link]

[23] E. C. Ike, *Late-Stage Geological Phenomena in the Zaria Basement Granites*, Precambrian Geology of Nigeria, Geological Survey of Nigeria, pp. 83-89, 1988. [Google Scholar] [Publisher Link]

[24] I. Garba, "Origin of Pan-African Mesothermal Gold Mineralisation at Bin Yauri, Nigeria," *Journal of African Earth Sciences*, vol. 31, no. 2, pp. 433-449, 2000. [CrossRef] [Google Scholar] [Publisher Link]

[25] Andongma W. Tende et al., "A Spatial Reconnaissance Survey for Gold Exploration in a Schist Belt," *Heliyon*, vol. 7, no. 11, pp. 1-15, 2021. [CrossRef] [Google Scholar] [Publisher Link]

[26] Fahad Abubakar et al., "Evaluation of Gold Mineralisation Potential Using AHP Systems and Weighted Overlay Analysis," *Scientific Reports*, vol. 14, pp. 1-20, 2024. [CrossRef] [Google Scholar] [Publisher Link]

[27] Robert Cullers, "Mineralogical and Chemical Changes of Soil and Stream Sediment Formed by Intense Weathering of the Danburg Granite, Georgia, U.S.A.," *Lithos*, vol. 21, no. 4, pp. 301-314, 1988. [CrossRef] [Google Scholar] [Publisher Link]

[28] Pramod Singh, "Major, Trace and REE Geochemistry of the Ganga River Sediments: Influence of Provenance and Sedimentary Processes," *Chemical Geology*, vol. 266, no. 3-4, pp. 242-255, 2009. [CrossRef] [Google Scholar] [Publisher Link]

[29] Tarasha Chitkara et al., "Geochemistry of the Bhor Saidan Alluvial Plains in Haryana State of North India: Implications for Catchment Weathering, Provenance, and Tectonic Setting," *Journal of Earth System Science*, vol. 132, 2023. [CrossRef] [Google Scholar] [Publisher Link]

[30] D.I Groves et al., "Orogenic Gold Deposits: A Proposed Classification in the Context of their Crustal Distribution and Relationship to other Gold Deposit Types," *Ore Geology Reviews*, vol. 13, no. 1-5, pp. 7-27, 1988. [CrossRef] [Google Scholar] [Publisher Link]

[31] S.K. Haldar, *Mineral Exploration: Principles and Applications*, Newnes, pp. 1-372, 2012. [Google Scholar] [Publisher Link]

[32] Samson Adeleke Oke, Akinlolu Festus Abimbola, and Dieter Rammlmair, "Mineralogical and Geochemical Characterization of Gold Bearing Quartz Veins and Soils in Parts of Maru Schist Belt Area, Northwestern Nigeria," *Journal of Geological Research*, vol. 2014, no. 1, pp. 1-17, 2014. [CrossRef] [Google Scholar] [Publisher Link]

[33] Dan J. Lapworth et al., "Geochemical Mapping Using Stream Sediments in West-Central Nigeria: Implications for Environmental Studies and Mineral Exploration in West Africa," *Applied Geochemistry*, vol. 27, no. 6, pp. 1053-1052, 2012. [CrossRef] [Google Scholar] [Publisher Link]

Appendix 1. Trace element composition of the stream sediment samples

Analyte Symbol	**Au (ppb)**	**Ag**	**As**	**Ba**	**Be**	**Co**	**Cr**	**Cs**	**Cu**	**Hf**	Ni	Pb	Rb	S	Sb	Sc
K1	< 5	< 0.5	< 2	145	< 1	1	10	< 0.5	8	2.2	4	7	< 20	0.003	< 0.2	0.4
K2	< 5	< 0.5	< 2	153	< 1	1	24	< 0.5	13	3.9	6	8	30	0.007	< 0.2	0.8
K3	< 5	< 0.5	< 2	189	< 1	1	14	< 0.5	7	6.2	5	11	< 20	0.003	< 0.2	0.9
K4	< 5	< 0.5	< 2	157	< 1	1	11	< 0.5	9	2.6	6	6	30	0.008	< 0.2	0.5
K5	< 5	< 0.5	< 2	216	< 1	< 1	12	< 0.5	10	4	5	10	40	0.003	< 0.2	0.8
K6	< 5	< 0.5	< 2	209	< 1	1	8	0.5	5	3.7	4	7	< 20	0.002	< 0.2	0.6
K7	< 5	< 0.5	< 2	226	< 1	< 1	20	< 0.5	7	7.2	5	10	< 20	0.003	< 0.2	0.8
K8	< 5	< 0.5	< 2	169	< 1	< 1	22	< 0.5	8	8.5	6	7	< 20	0.006	< 0.2	1.3
K9	< 5	< 0.5	< 2	430	3	37	112	8.2	10	3.9	49	26	190	0.005	< 0.2	18.3
K10	< 5	< 0.5	< 2	178	< 1	2	14	< 0.5	8	6.8	4	11	< 20	0.004	< 0.2	1.2
K11	< 5	< 0.5	< 2	147	1	4	35	2.7	19	5.4	14	9	30	0.002	< 0.2	5.4
K12	< 5	< 0.5	< 2	253	< 1	< 1	20	< 0.5	10	5.2	7	17	60	0.002	< 0.2	2.1
K13	< 5	< 0.5	< 2	212	< 1	< 1	19	< 0.5	6	6.3	6	8	30	0.006	< 0.2	1.1
K14	< 5	< 0.5	< 2	295	< 1	< 1	37	< 0.5	13	7.9	12	15	60	0.01	< 0.2	3.7
K15	< 5	< 0.5	< 2	500	1	9	48	0.5	5	5	15	16	90	0.003	< 0.2	5.7
K16	< 5	< 0.5	< 2	268	< 1	< 1	23	< 0.5	7	7.1	6	12	< 20	0.005	< 0.2	1.7
K17	< 5	< 0.5	< 2	136	< 1	< 1	37	< 0.5	24	6.2	5	12	< 20	0.003	< 0.2	1.5
K18	< 5	< 0.5	< 2	170	< 1	< 1	7	< 0.5	7	3.3	4	8	< 20	0.003	< 0.2	0.5
K19	< 5	< 0.5	< 2	286	< 1	3	16	< 0.5	7	9	7	13	< 20	0.002	0.2	2.2
K20	< 5	< 0.5	< 2	209	< 1	< 1	15	< 0.5	7	4.7	5	10	< 20	0.003	< 0.2	1.2
Min	-	-	-	136	1	1	7	0.5	5	2.2	4	6	30	0.002	0.2	0.4
Max	-	-	-	500	3	37	112	8.2	24	9	49	26	190	0.01	0.2	18.3
Mean	**-**	**-**	**-**	**227.4**	**1.67**	**6**	**25.2**	**2.975**	**9.5**	**5.455**	**8.75**	**11.15**	**62.22**	**0.004**	**0.2**	**2.54**
STD	-	-	-	92.04	0.94	10.60	22.60	3.15	4.60	1.89	9.75	4.55	49.17	0.0022	0	3.91
CCU	-	-	-	628	-	17.3	-	-	28	5.3	47	17	82	-	-	14

Appendix 2. Trace element composition of the stream sediment samples (continuation)

Analyte Symbol	Sr	Th	U	V	Y	Zn	Zr	Y	La	Ce	Nd	Sm	Eu	Tb	Yb	Lu
K1	22	1.5	< 0.5	7	4	8	70	4	6	11	< 5	1	< 0.1	< 0.5	0.4	0.1
K2	22	18.8	3.5	9	30	15	148	30	49.9	92	30	7.6	0.6	< 0.5	3.1	0.37
K3	27	31.7	4.3	10	48	11	266	48	85	161	62	13.3	0.6	0.6	4.8	0.67
K4	21	5.4	1.3	6	12	8	99	12	12.9	24	13	2.3	< 0.1	< 0.5	1.2	0.16
K5	31	13	2.8	7	20	12	153	20	38.6	72	31	5.8	0.2	< 0.5	1.6	0.2
K6	28	5.7	1.4	6	11	8	135	11	14.9	31	7	2.3	< 0.1	< 0.5	1.2	0.16
K7	31	29.4	7.1	6	45	9	287	45	79	149	57	12.2	0.7	0.6	3.8	0.5
K8	23	37.6	7.3	11	77	16	344	77	93.5	175	65	15.1	0.6	< 0.5	6.9	1.03
K9	27	12.3	4.2	94	63	116	144	63	58	114	71	12.7	1.9	< 0.5	5.5	0.8
K10	25	33.5	5.8	10	58	15	295	58	85.3	157	55	13.5	0.6	< 0.5	5.3	0.75
K11	11	16.2	4.2	36	18	41	217	18	43	72	29	6.6	0.5	< 0.5	1.5	0.29
K12	46	74.4	8.5	14	66	34	202	66	88	185	68	15.7	1	< 0.5	6.5	0.88
K13	31	32.4	4.2	12	34	15	268	34	59.6	124	48	9.8	1.1	< 0.5	3.9	0.48
K14	38	85.9	9.2	26	88	39	324	88	151	305	95	25.5	1.7	1	8.2	1.13
K15	80	40.7	4.2	32	50	35	202	50	80.9	165	48	12.4	1.4	< 0.5	4.7	0.77
K16	37	41.4	4.4	14	42	16	296	42	81.5	166	55	13.2	2	< 0.5	3.8	0.57
K17	19	137	15.2	11	184	17	240	184	266	534	186	44.8	2.7	1.9	18	2.36
K18	24	11.4	2	8	11	7	117	11	21.5	41	16	3.6	0.4	< 0.5	1.2	0.21
K19	35	45.9	5.5	17	55	18	361	55	95.7	198	70	15.1	2	< 0.5	5.3	0.73
K20	27	55.2	9.5	11	53	10	169	53	107	224	84	18.4	2.5	0.8	5.1	0.64
Min	11	1.5	1.3	6	4	7	70	**4**	**6**	**11**	**7**	**1**	**0.2**	**0.6**	**0.4**	**0.1**
Max	80	137	15.2	94	184	116	361	**184**	**266**	**534**	**186**	**44.8**	**2.7**	**1.9**	**18**	**2.36**
Mean	**30.25**	**36.47**	**5.51**	**17.35**	**48.45**	**22.5**	**216.85**	48.45	75.865	150	57.37	12.545	1.21	0.98	4.6	0.64
STD	13.65	31.77	3.29	19.43	38.65	23.88	83.75	38.65	56.17	114.13	38.29	9.50	0.76	0.48	3.73	0.49
CCU	320	10.5	2.7	97	-	67	193	**21**	**31**	**63**	**27**	**4.7**	**1**	**0.7**	**2**	**0.31**

Appendix 3. Major oxide element composition of the stream sediment samples

Analyte Symbol	R1	R2	R3	R4	R5	Min	Max	Mean	CCU
Au	< 5	< 5	< 5	< 5	< 5	-	-	-	
Ag	< 0.5	< 0.5	< 0.5	< 0.5	< 0.5	-	-	-	
As	< 2	< 2	< 2	< 2	< 2	-	-	-	
Ba	1400	208	120	10	432	10	1400	434	628
Be	3	3	2	< 1	< 1	2	3	2.666667	2.1
Bi	< 2	< 2	< 2	< 2	< 2	-	-	-	
Br	< 1	< 1	< 1	< 1	< 1	-	-	-	
Cd	< 0.5	< 0.5	< 0.5	< 0.5	< 0.5	-	-	-	
Co	9	23	< 1	3	4	3	23	9.75	17.3
Cr	< 1	65	15	11	8	8	65	24.75	92
Cs	< 0.5	0.9	< 0.5	< 0.5	< 0.5	0.9	0.9	0.9	4.9
Cu	15	10	19	18	9	9	19	14.2	28
Hf	15.6	5.1	< 0.5	< 0.5	< 0.5	5.1	15.6	10.35	5.3
Hg	< 1	< 1	< 1	< 1	< 1	-	-	-	
Ir	< 5	< 5	< 5	< 5	< 5	-	-	-	
Mo	< 2	< 2	< 2	< 2	< 2	-	-	-	
Ni	7	17	10	6	8	6	17	9.6	47
Pb	22	13	< 5	< 5	12	12	22	15.67	17
Rb	270	30	< 20	< 20	60	30	270	120.00	84
S	0.006	0.003	0.004	0.001	0.002	0.001	0.006	0.00	621
Sb	< 0.2	< 0.2	< 0.2	< 0.2	< 0.2	-	-	-	
Sc	9	19	0.9	0.4	1.2	0.4	19	6.10	14
Se	< 3	< 3	< 3	< 3	< 3	-	-	-	
Sr	301	431	72	< 2	60	60	431	216.00	320
Ta	< 1	< 1	< 1	< 1	< 1	-	-	-	
Th	30.4	8.8	3.4	0.9	1.7	0.9	30.4	9.04	10.5
U	< 0.5	4.4	< 0.5	< 0.5	< 0.5	4.4	4.4	4.40	2.7
V	39	121	10	< 5	8	8	121	44.50	97
W	< 3	< 3	< 3	< 3	< 3	-	-	-	
Zn	94	70	21	16	10	10	94	42.20	67
Zr	760	200	31	< 2	5	5	760	249.00	193
La	182	55	73.7	1.6	7.1	1.6	182	63.88	31
Ce	317	95	111	5	17	5	317	109.00	63
Nd	131	42	78	< 5	< 5	42	131	83.67	27
Sm	27.4	9.3	10.3	0.3	1.1	0.3	27.4	9.68	4.7
Eu	2.4	1.9	1.6	< 0.1	0.4	0.4	2.4	1.58	1.0
Tb	3.1	< 0.5	< 0.5	< 0.5	< 0.5	3.1	3.1	3.10	0.7
Y	63	32	7	< 1	4	4	63	26.50	21
Yb	5	3.3	0.9	< 0.1	0.5	0.5	5	2.43	1.96
Lu	0.68	0.5	0.11	< 0.05	< 0.05	0.11	0.68	0.43	0.31
LREE	630	192	262.7	6.6	24.1	6.6	630	223.08	
HREE	101.58	47	19.91	0.3	6	2	101.58	34.958	
REE total	731.58	239	282.61	6.9	30.1	6.9	731.58	258.038	
Mass	1.261	1.401	1.557	1.415	1.33	1.261	1.557	1.39	